PAPER

Shape-tunable two-dimensional assemblies from chromophore-conjugated crystallizable poly(L-lactides) with chain-length-dependent photophysical properties†

Chhandita Chakraborty, Aritra Rajak and Anindita Das [iD] *

This work reports temperature-dependent shape-changeable two-dimensional (2D) nanostructures by crystallization-driven self-assembly (CDSA) from a chromophore-conjugated poly(L-lactide) (PLLA) homo-polymer (**PTZ-P1**) that contained a polar dye, phenothiazine (PTZ), at the chain-end of the crystallizable PLLA. The CDSA of **PTZ-P1** in a polar solvent, isopropanol (iPrOH), by an uncontrolled heating−cooling process, majorly generates lozenge-shaped 2D platelets *via* chain-folding-mediated crystallization of the PLLA core, leading to the display of the phenothiazines on the 2D surface that confers colloidal stability and orange-emitting luminescent properties to the crystal lamellae. Isothermal crystallization at 60 °C causes a morphological change in **PTZ-P1** platelets from lozenge to truncated-lozenge to perfect hexagon under different annealing times, while no shape change was noticed in the structurally similar **PTZ-P2** polymer with a longer PLLA chain under similar conditions. This study unveils the complex link between the 2D platelet morphologies and degree of polymerization (DP) of PLLA and the corona-forming dye character. Further, the co-assembly potential of **PTZ-P1** with hydrophobic pyrene-termi-nated PLLAs of varying chain lengths (**PY-P1**, **PY-P2**, and **PY-P3**) was examined, as these two dyes could form a Förster Resonance Energy Transfer (FRET) pair on the 2D surface. The impact of the length of the crystallizable PLLA on the photophysical properties of the surface-occupied chromophores revealed crucial insights into interchromophoric interactions on the platelet surface. A reduction in the propensity for π-stacking with increasing chain-folding in longer PLLAs is manifested in the chain-length-dependent FRET efficiencies and excimer emission lifetimes within the resultant monolayered 2D assemblies. The unconventional "butterfly-shaped" molecular architecture of the tested phenothiazine, combined with its varied functional features and polar character, adds a distinctive dimension to the underdeveloped field of CDSA of chromophore-conjugated poly(L-lactides), opening future avenues for the development of advanced nanostructured biodegradable 2D materials with programmable morphology and optical functions.

Introduction

Ultrathin organic two-dimensional (2D) materials[1] of π-conjugated systems have attracted widespread attention due to their potential applications ranging from biomaterials[2a] to electronic devices.[2b] Due to the lack of effective and generally applicable strategies, controlling the shape, size, and mole-cular packing of many π-systems in two dimensions over a mesoscopic length scale represents a key challenge that dic-

tates their potential functional output. A promising strategy for creating various hierarchical and anisotropic structures, including 2D arrangements in semicrystalline block copoly-mers (BCPs), involves the use of an efficient "crystallization-driven self-assembly" (CDSA)[3] approach. In this process, chain-folding-mediated crystallization of the core-forming polymeric block in a corona-selective solvent compels the terminal corona-forming segment to locate on the 2D surface and provide colloidal stability. Thus far, the primary focus in this area has been to either customize the shapes of the nano-structures by playing with the relative volume fractions of the core- and/or corona-forming polymeric blocks or to precisely control the dimensions by a seeding approach called "living" CDSA,[3] which is analogous to the emerging living supramole-cular polymerization (LSP)[4] technique recently explored in

School of Applied and Interdisciplinary Sciences, Indian Association for the Cultivation of Science (IACS), 2A and 2B Raja. S.C. Mullick Road, Jadavpur, Kolkata-700032, India. E-mail: psuad2@iacs.res.in

†Electronic supplementary information (ESI) available. See DOI: https://doi.org/10.1039/d4nr01683a

functional π-systems. Manipulating the functional output from crystalline polymeric 2D nanostructures has captured the attention of the scientific community only in very recent times. Recently, we reported CDSA as an unconventional supramolecular bottom-up strategy for the fabrication of monolayered 2D assemblies of π-systems from different chromophore-conjugated poly(L-Lactide) (PLLA) homopolymers.[5] By judicially incorporating soluble corona-forming polar dyes such as naphthalene monoimide (NMI) or merocyanine (MC) at the chain-end of the crystallizable PLLA core in place of non-functional polymeric segments, we were successful in creating well-defined lozenge (diamond)-shaped crystalline lamellae with excellent colloidal stability and fluorescent properties in isopropanol (iPrOH). This is because the bulk solvent, due to its polar character, could effectively disperse the ordered 2D array of the polar dyes located on the platelet surface.[5] Furthermore, Förster resonance energy transfer (FRET)[5] properties could be achieved from the 2D surface of those crystalline nanosheets by incorporating suitable donor and acceptor FRET pairs. Despite our previous success in achieving predictable monolayered 2D assemblies of different π-systems, we were unable to control their shapes, unlike achievable in crystallizable BCPs, possibly due to the kinetically-driven crystallization process in the absence of a long solubilizing polymeric corona, leading to rigid and frozen structures. We anticipated that systematic variation in the polymer chain length in chromophore-appended PLLAs may offer exciting possibilities to tune their 2D morphology, as well as the photophysical properties of the surface-occupied terminal dyes by influencing their π-stacking, which is expected to be dependent on the extent of chain folding. In this work, we focus on investigating the role of different parameters such as temperature, chain length variation, and the character of the terminal dye on the crystallization kinetics, lamellae morphology, and photophysical properties in CDSA of chromophore-conjugated PLLA homopolymers.

We designed a new PLLA homopolymer (**PTZ-P1**) that featured a terminal phenothiazine (PTZ) dye as a soluble corona-forming moiety for the crystallizable PLLA core. Phenothiazine, a tricyclic heteroarene,[6] has been widely employed in organic transistors,[7] photovoltaics,[8] and light-emitting diodes.[9] It offers many advantages, such as extremely high hole mobility,[10] chemical stability,[11] and ease of functionalization at multiple positions.[12] Extensive research has focused on the solid-state properties of phenothiazine derivatives, particularly their unique optical and electronic properties and flexibility of functionalization. Unlike conventional planar π-scaffolds, the hierarchical self-assembly of phenothiazine in solutions,[13] particularly in two dimensions, is limited by its unique non-planar conformation characterized by a "butterfly" or bent-type structure.[6] Herein, we addressed this gap by leveraging the CDSA technique, which offered a tunable platform for studying phenothiazine's self-assembled properties. **PTZ-P1** could self-assemble into orange-emitting lozenge and truncated-lozenge-shaped 2D platelets by CDSA in iPrOH with monolayered thickness.[14] We demonstrated morphological transformation from diamond to regular hexagon by optimizing the crystallization temperature and annealing time, maintaining a narrow dispersity of 1.02 for **PTZ-P1**. Building on these findings, we extended our investigation on co-assemblies of **PTZ-P1** (acceptor) with pyrene-terminated PLLAs (donor) of different chain lengths (**PY-P1**, **PY-P2**, and **PY-P3**) to analyze their distance-dependent FRET properties. Our results reveal that the length of the donor chain has an unprecedented effect on the FRET response on the 2D surface. An increment in the FRET efficiency with a reduction in the donor chain length was observed, resulting in the highest achievable efficiency of ∼87% in **PTZ-P1** + **PY-P1** co-assembly.

Results and discussion

Synthesis of 2D platelets from phenothiazine-conjugated Poly (L-lactides)

In this study, a hydroxyl-functionalized phenothiazine (**PTZ-OH**) (Scheme 1 and S1†) serves as a potent initiator in the synthesis of poly(L-lactide), **PTZ-P1** by ring-opening polymerization (ROP). The size exclusion chromatography (SEC) showed a monomodal peak for **PTZ-P1** (Fig. S1†). All the characteristic peaks of PTZ could be seen in the ^{1}H-NMR spectrum of **PTZ-P1** in CDCl$_3$, which confirms the incorporation of the dye at the chain end of the homopolymer (Fig. S20 and Table S1†). From the end-group analysis, the degree of polymerization (DP) was determined to be 100, complying with the theoretical value. Next, the self-assembly of **PTZ-P1** was studied in iPrOH. An unimer solution of **PTZ-P1** in CHCl$_3$ was slowly evaporated to obtain a thin film. Subsequent addition of iPrOH and vigorous heating of the solution with a heat gun followed by spontaneous cooling and aging for 30 minutes directly resulted in discrete lozenge (diamond)-shaped and truncated-lozenge-shaped 2D structures with an average size of ≈2.34 μm, as shown in the atomic force microscopy (AFM) images (Fig. 1a and S2a†). The height profile showed a ∼8 nm thickness of the 2D platelets, closely corresponding to ∼32 repeating units.[15] This suggests the formation of monolayered crystalline lamellae, which is in agreement with previous reports where crystallization-driven self-assembly of PLLA is a contributing factor.[14,15b] No visual precipitation and structural homogeneity suggest appreciably high colloidal stability of the 2D platelets of **PTZ-P1** in iPrOH. This is conferred by the surface-occupied PTZ dye, which, by its intramolecular electronic conjugation, exhibits a high polar character that facilitates its solvation in the polar solvent iPrOH,[5a] where the PLLA core is insoluble. Transmission electron microscopy (TEM) analysis showed the formation of similar 2D platelets with comparable size (Fig. 1b). Furthermore, the highly crystalline nature of the diamond platelets was confirmed by the selected area electron diffraction (SAED) analysis (Fig. 1c).[14] The diffraction patterns reveal four (110) growth planes with d-spacings of 0.551 nm and two (200) planes with d-spacings of 0.557 nm. Similar diffraction spots have been previously reported for the solution-grown
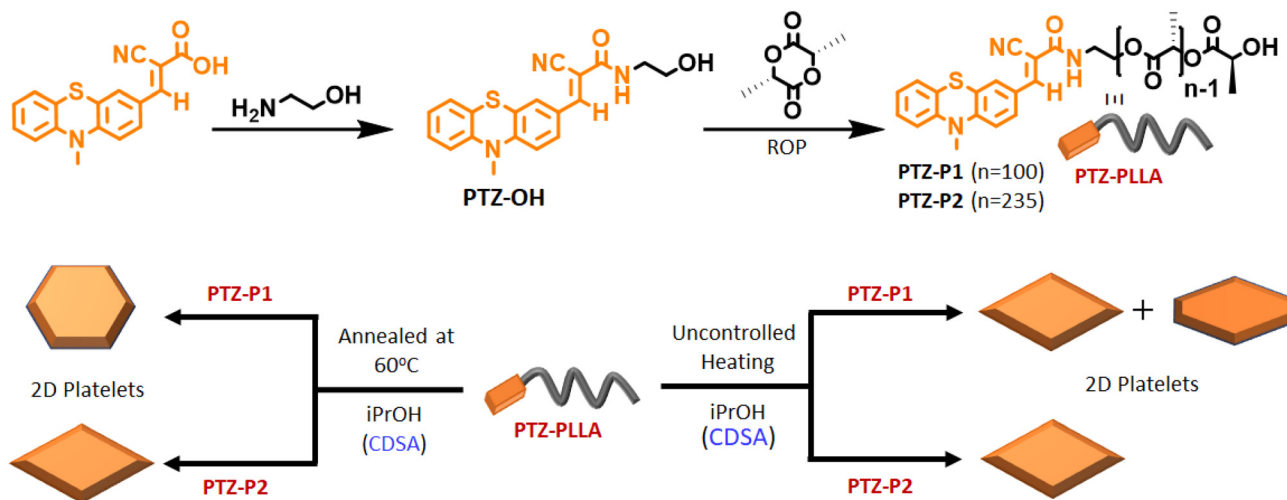
Scheme 1 Top: schematic representation of the synthesis of **PTZ-PLLA** by ROP; bottom: crystallization-driven self-assembly (CDSA) of poly(ʟ-lactide) homopolymers, **PTZ-P1** and **PTZ-P2** in isopropanol (iPrOH) under different conditions, and morphological modulation in **PTZ-P1** 2D platelets from a mixture of orange-emitting lozenge (diamond) and truncated-lozenge to hexagon.
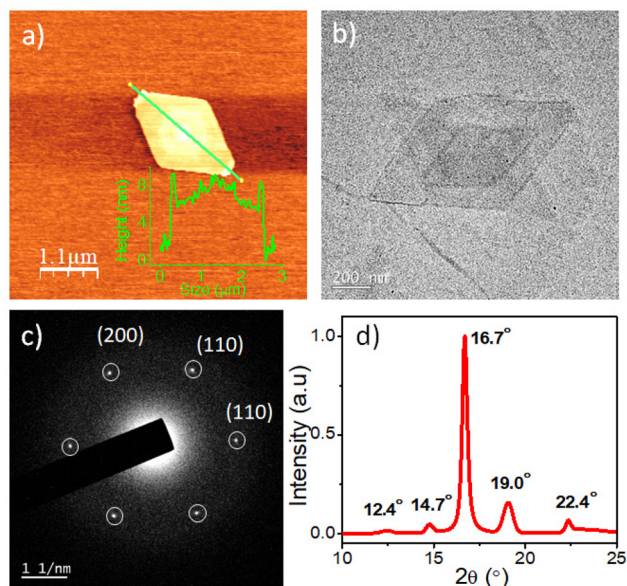

Fig. 1 (a) AFM image (inset: showing height profile of the 2D platelet) and (b) TEM image of the self-assembled diamond-shaped platelet of **PTZ-P1**; $C = 0.05$ mg mL^{-1}; (c) Selected area electron diffraction (SAED) patterns obtained from the diamond platelet of **PTZ-P1** in iPrOH; $C = 0.05$ mg mL^{-1}; (d) WAXRD of **PTZ-P1**. The powdered sample was prepared by slowly drying its self-assembled dispersion in iPrOH.

single crystals of PLLA and assigned to the orthorhombic α-form of PLLA.[14] The wide-angle X-ray scattering (WAXRD) analysis (Fig. 1d) of the PLLA powder obtained by a slow removal of the solvent revealed distinct peaks at $2\theta = 12.4°$ (103), 14.7° (010), 16.7° (110/200), 19.0° (203), and 22.4° (015), in accordance with the α-form of PLLA crystals.[5,14,16] Additionally, the differential scanning calorimetry (DSC) thermogram from solid **PTZ-P1** mass after removal of iPrOH, dis-

plays a single endothermic peak at 160 °C, corresponding to the melting point of the PLLA homocrystals (Fig. S3†).[5b,15,16d]

The terminally attached PTZ dye's fluorescent character additionally conferred luminescent properties to the crystalline PLLA platelets. Orange-emitting lozenge-shaped platelets, along with some truncated structures, could be clearly visualized by confocal laser scanning microscopy (CLSM) analysis (Fig. 2a and S2b†). The weight-average area (A_w) and number-average area (A_n) were measured to be 2.95 μm^2 and 2.86 μm^2, respectively, with a narrow dispersity of $A_w/A_n = 1.03$ (Fig. 2a and S2b†).[5,14ef] Corroborating with the CLSM analysis, **PTZ-P1**
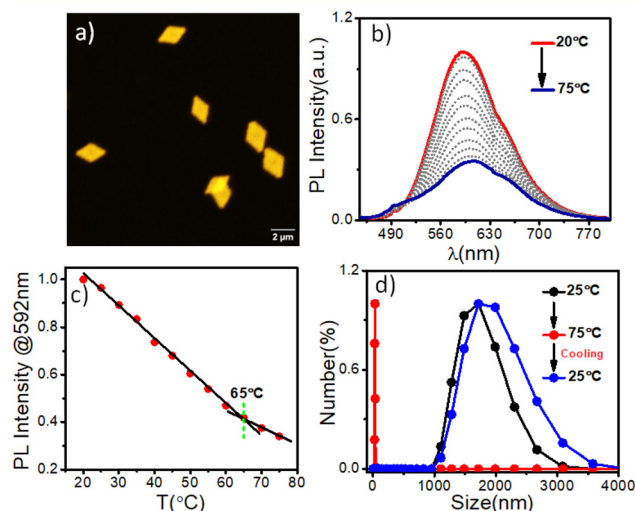

Fig. 2 (a) CLSM image of self-assembled **PTZ-P1** in iPrOH; $C = 0.05$ mg mL^{-1}; (b) Variable-temperature (VT) photoluminescence (PL) studies of **PTZ-P1** ($\lambda_{ex} = 430$ nm); excitation and emission slit = 2.5 nm/2.5 nm; (c) PL-Intensity vs. temperature plot from (b); (d) VT-DLS data of **PTZ-P1**; $C = 0.1$ mg mL^{-1}.

in iPrOH showed an emission band at λ_{em} = 592 nm (Fig. 2b), which is a result of high conjugation of the PTZ-chromophore due to its push–pull nature. The variable-temperature (VT) photoluminescence (PL) studies (Fig. 2b) demonstrate a sharp decrease in emission intensity with a rise in temperature, signifying the disassembly behavior of the 2D platelets. This trend continues until near saturation, marked by an inflection point at approximately 65 °C (Fig. 2c), denoted as the critical disassembly temperature of the 2D platelets. This is consistent with our recent findings on the disintegration temperature of other chromophore-functionalized PLLA diamond platelets in iPrOH.[5a] The enhanced emission at lower temperatures is attributed to the restricted motion of the fluorescent dyes in their confined 2D array. The dynamic light scattering (DLS) data (Fig. 2d) revealed a significant reduction in the aggregate size from ~2 μm to ~32 nm as the solution temperature was raised from 25 °C to 75 °C. This size reduction is consistent with the anticipated disassembly from the changes observed in the VT-PL studies. Interestingly, DLS analysis shows that the original size of the crystals can be restored upon cooling the solution back to 25 °C (Fig. 2d), indicating the reversible nature of the thermal disintegration process of the 2D platelets. The thermal disintegration of the 2D structures was further illustrated by capturing the CLSM images at 65 °C and

70 °C, which showed partial and complete disassembly, respectively (Fig. S5c–f†).

Morphological transformation

Next, we investigated the self-assembly of **PTZ-P1** crystallized isothermally at a higher temperature under different annealing conditions. For that, **PTZ-P1** in iPrOH was heated for 2 hours, 3 hours, and 4 hours at a constant temperature of 60 °C, subsequently cooled to room temperature, and then aged for 18 hours to allow the growth of single crystals. Notably, after annealing for 2 hours, the originally generated lozenge-shaped 2D platelets transformed into quasi hexagons and, after 3 hours and 4 hours, converted to nearly perfect hexagons with a very narrow dispersity of A_w/A_n = 1.02 (Fig. 3a–c and S4a–c†).[14a,c,17] Separately, we have observed that the lozenge-shaped platelets that were initially obtained from an uncontrolled heating–cooling process can also transform into hexagonal platelets upon annealing at 60 °C for 4 hours (Fig. S4d†). The AFM image (Fig. 3d) confirmed a monolayered hexagonal structure that was comparable in thickness (~7 nm) to the diamond-shaped crystalline lamellae generated from an uncontrolled heating–cooling process (Fig. 1a). However, the lamellae size (length between the two opposite vertices) increased from 2.5 μm to 4 μm with the change in
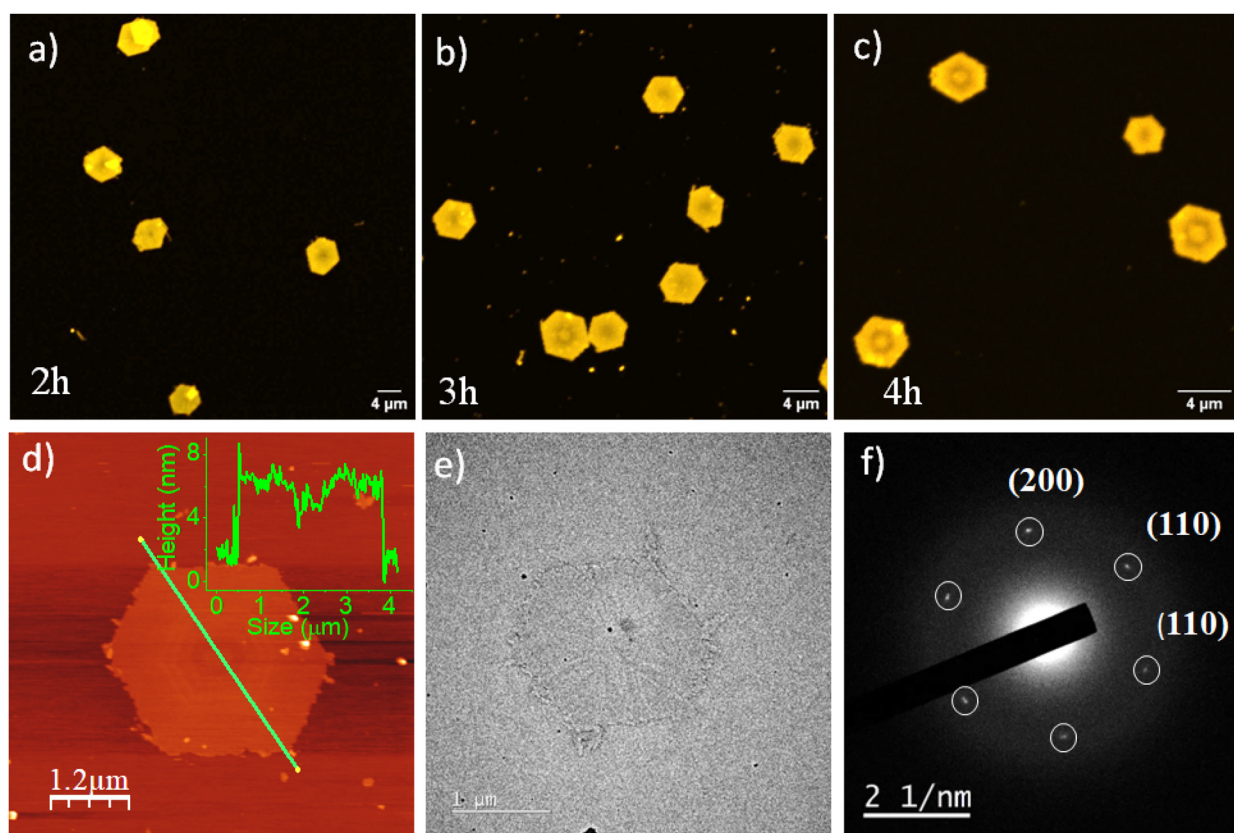

Fig. 3 CLSM images of single crystals of **PTZ-P1** homopolymer in iPrOH obtained at a constant nucleation temperature (60 °C) and varying annealing time as indicated in the figures: (a) t = 2 h; (b) t = 3 h; (c) t = 4 h; (d) AFM image and (e) TEM image of 4 h annealed sample of **PTZ-P1** in iPrOH at 60 °C; C = 0.05 mg mL^{-1}; (f) Selected area electron diffraction (SAED) patterns obtained from the hexagonal platelet of **PTZ-P1** in iPrOH; C = 0.05 mg mL^{-1}.

the crystal morphology (Fig. 1a and 3d). The SAED data collected from the hexagonal platelet (Fig. 3f) revealed comparable diffraction patterns to the lozenge-shaped platelets (Fig. 1c), indicating similar crystal structures.[14a,c] As a result, the hexagonal structures of **PTZ-P1** in iPrOH exhibit emission properties much like their diamond-shaped counterparts (Fig. S5a†), and both morphologies shared analogous disassembly temperatures as revealed from their VT-PL spectra (Fig. 2b and S5b†). Although less common, hexagonal-shaped crystals of PLLA are known to pack using both {110} and {100} growth planes and possess pseudo-hexagonal symmetry.[14a,c,17] In contrast, the growth faces of the lozenge-shaped crystals are the four {110} planes with chain-folding along the {110} direction. The competition between growth rates along the {100} and {110} planes determines the ultimate morphology of polymer crystals of PLLA. The emergence of the truncated-face {100 plane} in **PTZ-P1** crystals occurred during the uncontrolled heating–cooling crystallization process, and for truncated-lozenge structures, the {110} crystal planes grew faster than the {100} crystal planes. However, during isothermal crystallization at 60 °C, the truncation along the {100} crystal plane became active while the growth rate along the four {110} crystal planes diminished, and this process became more pronounced with increasing annealing time.[14a–c,17c] When the growth rates along the {100} and {110} crystal planes approached comparability, regular hexagons were formed from **PTZ-P1**, as seen after 3–4 hours of annealing. Consequently, the angles between all adjacent edges appear to be close to 120°. Thus, PLLA chains in hexagonal crystals correspond to those of the α-form with orthorhombic packing similar to its lozenge-shaped crystals.[14a–c,17c] This is also evidenced by the presence of comparable WAXRD (Fig. S6†) and SAED (Fig. 3f) patterns of **PTZ-P1** in these two unique 2D nanostructures. Such temperature-driven morphological transitions associated with polymer crystals are known to be caused by the diffusion-controlled change in chain mobility,[18] amongst many other parameters.[19] We have synthesized another PTZ-functionalized PLLA (**PTZ-P2**) with a longer chain length (DP = 235) while keeping other parameters unaltered. A dilute solution of **PTZ-P2** in iPrOH also produced diamond-shaped platelets by uncontrolled heating–cooling method, while its annealed sample at 60 °C for 4 hours did not exhibit any signs of truncation (Fig. S7a–c and S8a†). No morphological change in the case of the longer chain-length **PTZ-P2** (DP = 235) is explained by its slower diffusion-controlled mobility at 60 °C as compared to the shorter chain-length **PTZ-P1** (DP = 100) (Fig. S8a†). Our hypothesis was supported by the fact that when **PTZ-P2** was further heated to 80 °C for 4 hours, it gained some chain mobility to grow bigger crystals that show truncated faces (Fig. S8b–d†). However, after 20 hours of prolonged heating at 80 °C (Fig. S8e–g†), smaller-sized diamond platelets were regenerated, possibly resulting from the dissolution of the PLLA chains from the edges of the initially formed bigger crystals. This suggests an optimal annealing temperature and time are essential for crystal growth and its morphological transition.

Chain-length variation: impact on 2D morphology and photophysical properties of pyrene-conjugated poly(L-lactides)

We envisaged that the CDSA approach offers a unique advantage in investigating the chain-length-dependent FRET responses from the 2D surface of the co-assembled nanostructures, which had not been investigated earlier. We anticipated that pyrene could participate as an efficient FRET donor for the tested phenothiazine acceptor due to their required spectral overlap (Fig. S9†). With this objective, we synthesized pyrene-appended PLLAs, *i.e.*, **PY-P1**, **PY-P2**, and **PY-P3**, with DPs of 93, 245, and 800, respectively (Table S1†), by ROP of L-lactide using **PY-OH** as an initiator. A monomodal peak was observed for all the pyrene derivatives in THF in size-exclusion chromatography (SEC) with a moderate dispersion of 1.3–1.4 (Fig. 4b).[5a] Before investigating the FRET properties in the co-assemblies, we first studied the impact of chain-length variation on the self-assembly of **PY-P1**, **PY-P2**, and **PY-P3**. All
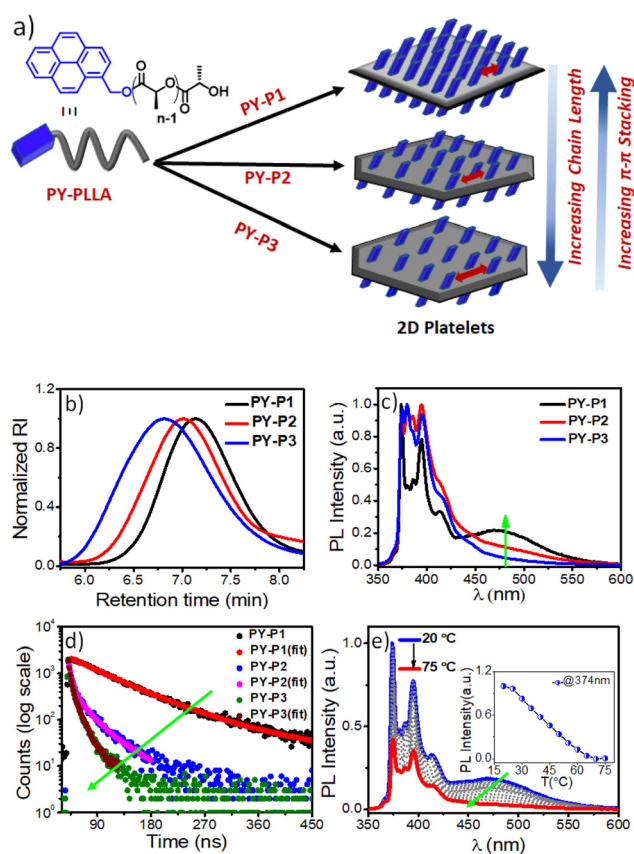

Fig. 4 (a) Schematic diagram of homocrystals of **PY-PLLA** with three different chain length; (b) SEC plots of **PY-P1**, **PY-P2** and **PY-P3** in THF; (c) Photoluminescence (PL) spectra (normalized) of **PY-P1**, **PY-P2** and **PY-P3** in iPrOH; λ_{ex} = 337 nm, C = 0.1 mg mL^{-1}; (d) Time-resolved fluorescence decay profiles of **PY-P1**, **PY-P2** and **PY-P3** at 472 nm (λ_{ex} = 337 nm); (e) Changes in the emission spectra of self-assembled **PY-P1** in iPrOH as a function of temperature; Inset: plot of the **PY-P1** emission intensity (λ_{em} = 374 nm) *vs.* temperature, C = 0.1 mg mL^{-1}, pathlength = 10 mm, excitation and emission slit = 1 nm/1 nm; λ_{ex} = 337 nm.

pyrene-conjugated PLLAs produced 2D platelets that show poor colloidal stability and tend to precipitate in iPrOH after a few hours, in contrast to the stable and uniform structures seen in the case of PLLAs chain-terminated with polar dyes like phenothiazine and previously studied NMI or merocyanines.[5a] A dilute solution of PY-P1, PY-P2, and PY-P3 produced crystalline lamellae of diamond, truncated-diamond, and pseudo-hexagon shapes (Fig. S10†), respectively, indicating that longer pyrene-end-capped PLLA chains are more prone to truncation due to the faster growth along {100} planes.[15b] It is interesting to note that the morphology of the 2D platelets generated from CDSA of the phenothiazine-functionalized PLLAs showed a reverse trend as compared to the previous literature knowledge on block copolymers of enantiopure polylactides[15b] and our own findings with hydrophobic pyrene-end-capped PLLAs, i.e. the platelet morphology of PTZ-P2 with longer PLLA chains shows no sign of truncation at ambient temperature or even at 60 °C, unlike the shorter one. In CDSA of block copolymers, the ultimate morphology is governed by many factors like polymer composition, structure of the corona, solvent-corona interactions, the presence of cosolvent, and different self-assembly conditions.[3,14] For CDSA of the chromophore-conjugated PLLAs with small molecule-based corona (where the steric component is minimal), under a given condition in a particular solvent, the crystallization kinetics will be dictated by both the corona solvation and degree of core crystallization, which are likely to be influenced by the nature of the terminal chromophore and the crystallizable polymer chain length, respectively. As the extent of interaction between the corona-forming dye and the polar solvent (iPrOH) will be different for phenothiazine (polar) and pyrene (nonpolar), the repeating unit variation does not exert the same impact on the polymer crystallization kinetics in the CDSA of these two types of chromophore-conjugated PLLAs. Thus, our results unravel the remarkable role that a single corona-forming π-scaffold has in CDSA, which goes beyond stabilizing the 2D structure and conferring it with distinct surface properties. The terminal dye plays a pivotal role in the crystallization process and crystal shape, which is comparable to the impact of solvent-selective non-crystallizable polymeric segments in the CDSA of block copolymers.

Pyrene, a spatially sensitive probe, exhibits an excimer band at ∼472 nm when two fluorophores are in close spatial proximity, in addition to monomeric fluorescence emission peaks (373–405), and the excimer band intensity depends on the distance of separation between the pyrenes and the π–π overlap.[20] As the density of the corona-forming segment on the platelet surface is dependent on the length of the polymer chain, we anticipated that the increased number of chain-folding in higher DP PLLA will reduce the surface density of pyrene, leading to less probable spatial proximity of the chromophores for π-stacking interactions on the 2D surface as compared to the PLLA with shorter chain length. This can be manifested by comparing the excimer/monomer (e/m) ratio in the three polymers PY-P1, PY-P2, and PY-P3. The emission spectrum of PY-P1 exhibited a broad excimer

band at 472 nm (Fig. 4c), attributed to π-stacking interactions among the terminally-linked pyrenes.[20] The excimer band was notably reduced in PY-P2 and became almost negligible in PY-P3, suggesting a chain length-dependent phenomenon. This is apparent from the e/m ratio that follows the trend PY-P1 (0.23) > PY-P2 (0.12) > PY-P3 (0.05).[21] Time-correlated single photon counting (TCSPC) studies further confirmed this, revealing a drastic reduction in the excimer band lifetime[22] from 100.00 ns to 25.85 ns to 8.40 ns for PY-P1, PY-P2, and PY-P3 respectively (Fig. 4d and Table S3†), indicative of insignificant π–π-interactions in PY-P2 and PY-P3. To validate our hypothesis and eliminate any changes caused by intrinsic differences in the dye concentration in these three polymers, we conducted a control experiment with the free dye (PY-OH) at a concentration equivalent to the pyrene concentration in PY-P1 (Fig. S11†). Under the same conditions, no excimer band was observed from the dye without the polymer chain (Fig. S11†), emphasizing that the π-stacking of pyrene in iPrOH and subsequent excimer band formation were an outcome of the CDSA. In further investigations, we conducted a dilution experiment in iPrOH using chloroform (CHCl₃) as a good solvent for disassembly of the preformed 2D platelets of PY-P1. The gradual addition of CHCl₃ resulted in a reduction in the intensity of the excimer band. Notably, with 33% CHCl₃, the excimer emission completely disappeared, affirming that it originates from the 2D platelets obtained through CDSA (Fig. S12†). VT-photoluminescence studies reveal similar results. As temperature ascends from 20 °C to 75 °C, the excimer band progressively diminishes for PY-P1. The monomer band intensity (λ = 374 nm) vs. temperature plot reveals a consistent disassembly temperature of 70 °C for PY-P1 (Fig. 4e), closely matching the disassembly temperature observed for PY-P2 and PY-P3 (Fig. S13b–d†), as well as PTZ-P1 (Fig. 2c). This synchronized disassembly behavior across different dye-appended PLLAs underscores the thermal sensitivity of these 2D structures across varying tested chain lengths.

Chain-length variation: impact on FRET response in two-component 2D assemblies

Next, we wanted to explore the impact of polymer chain-length variation on the FRET properties in two-component CDSA of PTZ-P1 polymer with pyrene-functionalized PY-P1, PY-P2, and PY-P3 having different repeating units. Two-dimensional co-assemblies of PY-P1, PY-P2, and PY-P3 with PTZ-P1 prepared by following the previously mentioned uncontrolled heating–cooling process in iPrOH were assigned as CoAs-1, CoAs-2, CoAs-3 respectively. The CLSM images (Fig. 5) unveiled majorly truncated lozenge-shaped platelets with morphological consistency across all tested co-assembled structures (CoAs-1, CoAs-2, and CoAs-3) and emitting in blue and orange under selective excitation at their respective wavelengths. Intriguingly, the perfect overlay of the two distinct colors in the merged image revealed dual emission (Fig. 5) from the crystalline 2D lamellae. This transformation provided clear evi-
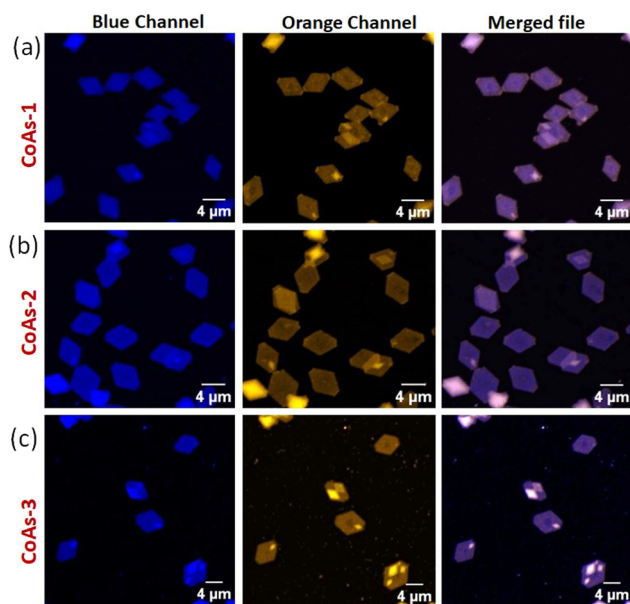
Fig. 5 CLSM images of co-assembly of (a) **PY-P1** + **PTZ-P1** (**CoAs-1**); (b) **PY-P2** + **PTZ-P1** (**CoAs-2**), and (c) **PY-P3** + **PTZ-P1** (**CoAs-3**); [**PY-P1**] = [**PY-P2**] = [**PY-P3**] = [**PTZ-P1**] = 0.05 mg mL^{-1}.

dence of the co-localization of the two dyes (PY and PTZ) on the platelet surface. While the CLSM investigation offered visual confirmation of the presence and co-localization of the two chromophores on the surface of the 2D crystallites, we relied upon FRET studies to obtain valuable information about the spatial interaction between the donor and acceptor dyes. Remarkably, we noted a substantial overlap between the absorption spectrum of **PTZ-P1** and the emission spectrum of **PY-P1**, establishing them as a FRET pair (Fig. S13a†), laying the foundation for further exploration of the chain-length dependent FRET properties within the three studied systems, *i.e.*, **CoAs-1**, **CoAs-2**, and **CoAs-3**. As FRET is highly sensitive to the distance between the two communicating dyes (which has to be within 10 nm),[22a,23] we envisaged that for the same FRET pair, the energy transfer efficiency can be tuned by varying the distance between the dyes through alteration in the PLLA chain length. Upon photoexcitation of **CoAs-1** at the absorption wavelength of the donor **PY-P1** (λ_{ex} = 337 nm), we observed quenching in the pyrene emission (λ_{em} = 374 nm) with complete disappearance of the excimer band (Fig. 6b). Intriguingly, this was accompanied by a 5-fold enhancement in the emission intensity of the acceptor **PTZ-P1** (λ_{em} = 592 nm) compared to the direct acceptor emission at λ_{ex} = 337 nm (Fig. 6b). An impressively high FRET efficiency ($E = 1 - I_{DA}/I_D$) of 88% was observed (Fig. 6b), where I_{DA} and I_D represent the emission intensity of **PY-P1** (λ_{em} = 374 nm) in the presence and absence of the **PTZ-P1** acceptor, respectively. This was validated by the fluorescence lifetime measurement by time-correlated single photon counting (TCSPC) experiments (Fig. 6c).[22] The average lifetime of the donor dye in **PY-P1** (λ_{ex} = 280 nm) was deter-

mined to be τ_D = 109.91 ns. Significantly, its lifetime was markedly reduced to 14.64 ns (τ_{DA}) within the **CoAs-1** (Table S2†), providing clear evidence of energy transfer from **PY-P1** to **PTZ-P1**. The energy transfer efficiency ($E = 1 - \tau_{DA}/\tau_D$) from the lifetime measurements (Fig. 6c) yielded a value of ∼87% complementing with the steady-state data, where τ_{DA} and τ_D represent the lifetime of pyrene in **PY-P1** (λ_{em} = 374 nm) in the presence and absence of the **PTZ-P1** polymer, respectively. To further probe that the FRET originating from the 2D surface is a consequence of the CDSA of the PLLA chain, we conducted a dilution experiment in **CoAs-1** using a corona-selective cosolvent, CHCl$_3$. With the gradual addition of CHCl$_3$ (v/v) in iPrOH, the emission intensity of **PTZ-P1** in **CoAs-1** decreased concurrently with an increase in the **PY-P1** emission (Fig. 6f and g). The disappearance of FRET, indicated by the alteration in emission intensities, upon the addition of CHCl$_3$ further confirmed the sensitivity of these crystalline lamellae to the presence of a good solvent, leading to the disruption of the organized chromophore assembly. Additionally, we explored the effect of temperature on the FRET response, which is expected to be dependent on the thermal stability of the 2D structures. With a gradual increase in temperature from 25 °C to 75 °C, FRET started diminishing in **CoAs-1** and completely ceased above 70 °C, suggesting temperature-dependent disassembly of the 2D platelets (Fig. 6d and e). This study further underscores the occurrence of nonradiative energy transfer from the donor to the acceptor polymer on the surface of the 2D co-platelet with reasonably high thermal stability. To investigate any effect of variation in the donor polymer chain length on the FRET response, similar studies were performed with **CoAs-2** and **CoAs-3** (Fig. S14 and S15†). A reduction in the average lifetime of **PY-P2** in **CoAs-2** from 74.65 ns to 22.52 ns and **PY-P3** in **CoAs-3** from 73.10 ns to 33.00 ns (Fig. S14a, b and Table S2†) validated similar energy transfer processes occurring in **CoAs-2** (∼70%) and **CoAs-3** (∼55%), however, with reduced efficiencies as compared to **CoAs-1** (∼87%). A reverse correlation of the FRET efficiency and excimer formation (Fig. 4a and c) with respect to the ascending donor chain length going from **PY-P1** to **PY-P2** to **PY-P3** can be attributed to the diminishing interchromophoric interactions on the 2D surface. The extended spatial distance induced by longer polymer chains creates a less favorable environment for close proximity and intimate interaction between the donor and acceptor chromophores, resulting in a decreased probability of energy transfer events in **CoAs-2** and **CoAs-3**. We conducted further assessments by measuring the FRET distances[24] in **CoAs-1** (1.98 nm), **CoAs-2** (2.23 nm), and **CoAs-3** (2.46 nm), which align with the proposed hypothesis. Further, the temperature- and cosolvent-dependent FRET studies reveal that all three donor–acceptor co-assembled 2D platelets exhibit comparable thermal stability and complete disassembly above 70 °C (Fig. S15c†) or ∼33% CHCl$_3$ addition (Fig. 6g). However, the tolerance for the cosolvent becomes slightly higher as the donor chain length increases in the two-component 2D platelets (Fig. 6g).
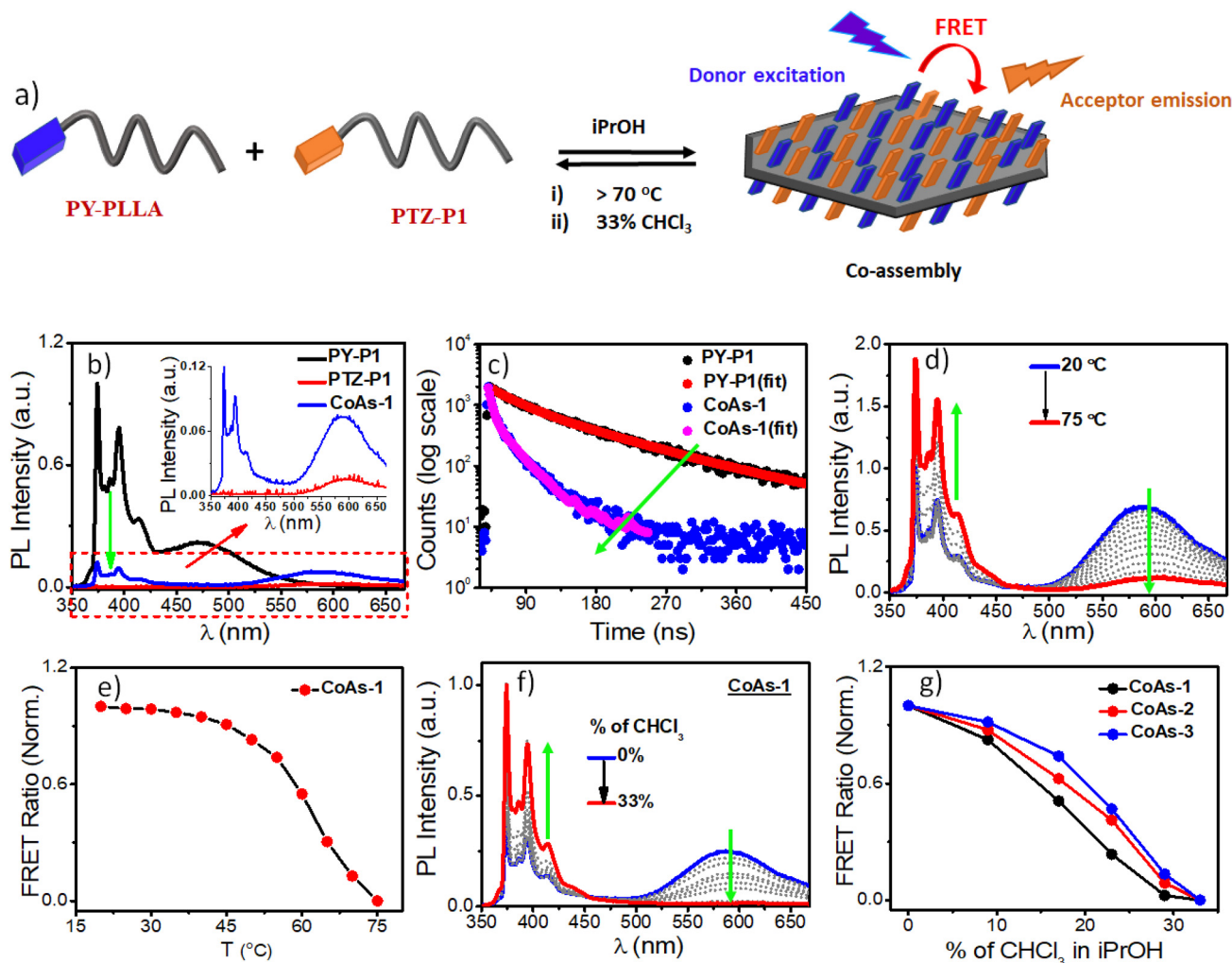
Fig. 6 (a) A schematic demonstration of Förster Resonance Energy Transfer (FRET) in crystallization-driven co-assembly of **PY-PLLA** and **PTZ-P1** on the surface of 2D platelets; (b) Emission spectra of **PY-P1**, **PTZ-P1** and their 1:1 co-assembly in iPrOH; λ_{ex} = 337 nm, slit = 1 nm/1 nm; (c) Time-resolved fluorescence decay profiles of **PY-P1** and (1:1) **PY-P1** + **PTZ-P1** co-assembly (**CoAs-1**); (d) Variable-Temperature (VT) PL studies of **CoAs-1** (λ_{ex} = 337 nm, slit = 1.5 nm/1.5 nm) from 20 °C to 75 °C, 5° interval; (e) Plot of FRET ratio of **CoAs-1** as a function of temperature (normalized); (f) Changes in the emission spectra of 1:1 **PY-P1** + **PTZ-P1** co-assembly (**CoAs-1**) in iPrOH as a function of CHCl₃ addition; λ_{ex} = 337 nm, slit = 1.5 nm/ 1.5 nm; (g) Plot of FRET ratio ($I_A/I_A + I_D$) vs. % of CHCl₃ in iPrOH, where I_A and I_D represent emission of **PTZ-P1** (λ_{em} = 592 nm) and **PY-P1**, **PY-P2**, and **PY-P3** (λ_{em} = 374 nm), respectively.

Conclusions

In summary, crystallization-driven self-assembly (CDSA) from dipolar phenothiazine end-capped poly(L-lactide) (PLLA) homopolymers (**PTZ-P1**/**PTZ-P2**) has been demonstrated in iPrOH. This results in colloidally stable discrete and mono-layered, lozenge-shaped, and truncated-lozenge-shaped 2D platelets with surface-decorated phenothiazine dyes, leading to previously unexplored orange emission from the 2D structures. Notably, a temperature-dependent morphological transition from lozenge-shaped 2D platelets to perfect hexagons could be achieved with structural precision and narrow dispersion (1.02) in the shorter chain length **PTZ-P1**. Furthermore, we examined the potential effects of introducing pyrene (donor), a second dye with a FRET relationship with the phenothiazine

(acceptor) moiety being studied, on the surface properties of the resulting crystalline 2D platelets. An important under-standing of the correlation between the crystallizable PLLA chain length and the spatial proximity of the surface-occupied chromophores for π-stacking was gained by studying the effects of varying degrees of polymerization in **PY-P1**, **PY-P2**, and **PY-P3** on the excimer emissions in their respective homo-platelets and FRET efficiencies in the co-platelets (**CoAs-1**, **CoAs-2**, and **CoAs-3**) with **PTZ-P1**, which is a significant new development in CDSA of chromophore-conjugated crystalliz-able polymers. Furthermore, we showed that the 2D platelet morphology depends not only on external factors like tempera-ture and annealing times in a specific crystallizable solvent (iPrOH) but also on intrinsic structural parameters like the length of the PLLA chain and the nature of the corona-forming

terminal π-scaffold, which potentially influence the unimer-to-nuclei ratio through varying degrees of corona-solvent interactions. This knowledge enriches our toolbox for generating distinct hierarchical 2D assemblies of π-conjugated systems with consistent properties by controlling different crystallization parameters in PLLA scaffolds. Overall findings of this work advance our understanding of the intricate correlation between chemical structure, supramolecular assembly, and resulting photophysical attributes in CDSA of chromophore-conjugated crystallizable poly(L-lactides), demonstrating its potential as a versatile tool for the design and engineering of functional biodegradable 2D materials with customized optical behaviors from structurally diverse π-systems.

Author contributions

C. C. carried out the synthesis and characterization of the polymers and conducted the experiments. C. C. and A. R. analyzed the data. All authors contributed to the manuscript preparation. A. D. conceptualized the project, raised research funding, and supervised the entire work. All authors have approved the final version of the manuscript.

Data availability

The data supporting this article have been included as part of the ESI.†

Conflicts of interest

There are no conflicts to declare.

Acknowledgements

References

1 (a) G. Fernández, F. García, F. Aparicio, E. Matesanz and L. Sánchez, *Chem. Commun.*, 2009, 7155; (b) F. Yang, S. Cheng, X. Zhang, X. Ren, R. Li, H. Dong and W. Hu, *Adv. Mater.*, 2018, **30**, 1702415; (c) A. D. Merg, E. van Genderen, A. Bazrafshan, H. Su, X. Zuo, G. Touponse, T. B. Blum, K. Salaita, J. P. Abrahams and V. P. Conticello, *J. Am. Chem. Soc.*, 2019, **141**, 20107; (d) R. R. Liang, S. Y. Jiang, R. Han A and X. Zhao, *Chem. Soc. Rev.*, 2020, **49**, 3920.

2 (a) X. Zhang, C. Gong, O. U. Akakuru, Z. Su, A. Wu and G. Wei, *Chem. Soc. Rev.*, 2019, **48**, 5564; (b) M. C. Lemme, D. Akinwande, C. Huyghebaert and C. Stampfer, *Nat. Commun.*, 2022, **13**, 1392.

3 (a) S. Agbolaghi, S. Abbaspoor and F. Abbasi, *Prog. Polym. Sci.*, 2018, **81**, 22; (b) S. Ganda and M. H. Stenzel, *Prog. Polym. Sci.*, 2020, **101**, 101195; (c) L. MacFarlane, C. Zhao, J. Cai, H. Qiu and I. Manners, *Chem. Sci.*, 2021, **12**, 4661; (d) C. Yang, Z.-X. Li and J.-T. Xu, *J. Polym. Sci.*, 2022, **60**, 2153; (e) Y. Cha, C. Jarrett-Wilkins, M. A. Rahman, T. Zhu, Y. Sha, I. Manners and C. Tang, *ACS Macro Lett.*, 2019, **8**, 835; (f) X. Wang, G. Guerin, H. Wang, Y. Wang, I. Manners and M. A. Winnik, *Science*, 2007, **317**, 644; (g) H. Qiu, Y. Gao, C. E. Boott, O. E. Gould, R. L. Harniman, M. J. Miles, S. E. Webb, M. A. Winnik and I. Manners, *Science*, 2016, **352**, 697; (h) T. Xia, Z. Tong, Y. Xie, M. C. Arno, S. Lei, L. Xiao, J. Y. Rho, C. T. J. Ferguson, I. Manners, A. P. Dove and R. K. O'Reilly, *J. Am. Chem. Soc.*, 2023, **145**, 25274; (i) Xu Zhang, G. Chen, L. Liu, L. Zhu and Z. Tong, *Macromolecules*, 2022, **55**, 8250.

4 (a) S. Ogi, K. Sugiyasu, S. Manna, S. Samitsu and M. Takeuchi, *Nat. Chem.*, 2014, **6**, 188; (b) R. D. Mukhopadhyay and A. Ajayaghosh, *Science*, 2015, **349**, 241; (c) J. Kang, D. Miyajima, T. Mori, Y. Inoue, Y. Itoh and T. Aida, *Science*, 2015, **347**, 646; (d) W. Wagner, M. Wehner, V. Stepanenko, S. Ogi and F. Würthner, *Angew. Chem., Int. Ed.*, 2017, **56**, 16008; (e) S. Yagai, Y. Kitamoto, S. Datta and B. Adhikari, *Acc. Chem. Res.*, 2019, **52**, 1325; (f) J. Matern, Y. Dorca, L. Sánchez and G. Fernández, *Angew. Chem., Int. Ed.*, 2019, **58**, 16730; (g) G. Ghosh, S. Dey and S. Ghosh, *Chem. Commun.*, 2020, **56**, 6757; (h) B. Adelizzi, N. J. Van Zee, L. N. J. de Windt, A. R. A. Palmans and E. W. Meijer, *J. Am. Chem. Soc.*, 2019, **141**, 6110; (i) A. Sarkar, R. Sasmal, C. Empereur-mot, D. Bochicchio, S. V. K. Kompella, K. Sharma, S. Dhiman, B. Sundaram, S. S. Agasti, G. M. Pavan and S. J. George, *J. Am. Chem. Soc.*, 2020, **142**, 7606; (j) P. Khanra, A. K. Singh, L. Roy and A. Das, *J. Am. Chem. Soc.*, 2023, **145**, 5270; (k) P. Khanra, P. Rajdev and A. Das, *Angew. Chem., Int. Ed.*, 2024, e202400486; (l) H. Itabashi, K. Tashiro, S. Koshikawa, S. Datta and S. Yagai, *Chem. Commun.*, 2023, **59**, 7375.

5 (a) A. Rajak and A. Das, *Angew. Chem., Int. Ed.*, 2022, **61**, e20211657; (b) A. Rajak and A. Das, *Angew. Chem., Int. Ed.*, 2023, **62**, e2023142.

6 (a) J. Bell, J. Blount, O. Briscoe and H. Freeman, *Chem. Commun.*, 1968, 1656; (b) S. P. Massie, *Chem. Rev.*, 1954, **54**, 797; (c) P. S. Gangadhar, G. Reddy, S. Prasanthkumar and L. Giribabu, *Phys. Chem. Chem. Phys.*, 2021, **23**, 14969.

7 W. Zhou, Y. Wen, L. Ma, Y. Liu and X. Zhan, *Macromolecules*, 2012, **45**, 4115.

8 S. Zimosz, A. Slodek, P. Gnida, A. Glinka, M. Ziółek, D. Zych, A. K. Pająk, M. Vasylieva and E. Schab-Balcerzak, *J. Phys. Chem. C*, 2022, **126**, 8986.

9 J. K. Salunke, F. L. Wong, K. Feron, S. Manzhos, M. F. Lo, D. Shinde, A. Patil, C. S. Lee, V. A. L. Roy, P. S. Prakash and P. Wadgaonkar, *J. Mater. Chem. C*, 2016, **4**, 1009.

10 (*a*) K. D. Thériault and T. C. Sutherland, *Phys. Chem. Chem. Phys.*, 2014, **16**, 12266; (*b*) S. Thokala and S. P. Singh, *ACS Omega*, 2020, **5**, 5608.

11 L. M. Sigmund, F. Ebner, C. Jöst, J. Spengler, N. Gönnheimer, D. Hartmann and L. Greb, *Chem. – Eur. J.*, 2020, **26**, 3152.

12 (*a*) Y. Rout, A. Ekbote and R. Misra, *J. Mater. Chem. C*, 2021, **9**, 7508; (*b*) S. Revoju, A. Matuhina, L. Canil, H. Salonen, A. Hiltunen, A. Abate and P. Vivo, *J. Mater. Chem. C*, 2020, **8**, 15486.

13 (*a*) C. Arivazhagan, S. Satapathy, A. Jana, P. Malakar, E. Prasad and S. Ghosh, *Chem. – Eur. J.*, 2018, **24**, 13213; (*b*) J. Gong, M. Yu, C. Wang, J. Tan, S. Wang, S. Zhao, Z. Zhao, A. Qin, B. Tang and X. Zhang, *Chem. Commun.*, 2019, **55**, 10768; (*c*) S. Suganya, K. Debsharma, E. Ravindran, M. Mahato and E. Prasad, *ACS Appl. Polym. Mater.*, 2020, **2**, 1222; (*d*) N. V. Lakshmi, T. M. Babu and E. Prasad, *Chem. Commun.*, 2016, **52**, 617.

14 (*a*) T. Iwata and Y. Doi, *Macromolecules*, 1998, **31**, 2461; (*b*) J. X. Zheng, H. Xiong, W. Y. Chen, K. Lee, R. M. V. Horn, R. P. Quirk, B. Lotz, E. L. Thomas, A.-C. Shi and S. Z. D. Cheng, *Macromolecules*, 2006, **39**, 641; (*c*) J. Yang, T. Zhao, Y. Zhou, L. Liu, G. Li, E. Zhou and X. Chen, *Macromolecules*, 2007, **40**, 2791; (*d*) M. Inam, G. Cambridge, A. P. Barry, Z. P. L. Laker, N. R. Wilson, R. T. Mathers, A. P. Dove and R. K. O'Reilly, *Chem. Sci.*, 2017, **8**, 4223; (*e*) X. He, Y. He, M. S. Hsiao, R. L. Harniman, S. Pearce, M. A. Winnik and I. Manners, *J. Am. Chem. Soc.*, 2017, **139**, 9221; (*f*) X. He, M. S. Hsiao, C. E. Boott, R. L. Harniman, A. Nazemi, X. Li, M. A. Winnik and I. Manners, *Nat. Mater.*, 2017, **16**, 481; (*g*) H. Qi, H. Zhou, Q. Tang, J. Y. Lee, Z. Fan, S. Kim, M. C. Staub, T. Zhou, S. Mei, Lin Han, D. J. Pochan, H. Cheng, W. Hu and C. Y. Li, *Nat. Commun.*, 2018, **9**, 3005; (*h*) M. Inam, J. R. Jones, M. M. Pérez-Madrigal, M. C. Arno, A. P. Dove and R. K. O'Reilly, *ACS Cent. Sci.*, 2018, **4**, 63; (*i*) W. Yu, M. Inam, J. R. Jones, A. P. Dove and R. K. O'Reilly, *Polym. Chem.*, 2017, **8**, 5504.

15 (*a*) B. A. G. Lamers, B. Van Genabeek, J. Hennissen, B. F. M. De Waal, A. R. A. Palmans and E. W. Meijer, *Macromolecules*, 2019, **52**, 1200; (*b*) Y. Kwon and K. T. Kim, *Macromolecules*, 2021, **54**, 10487.

16 (*a*) M. L. Di Lorenzo and R. Androsch, *Polym. Int.*, 2019, **68**, 320; (*b*) Z. Li, Y. Zhang, L. Wu, W. Yu, T. R. Wilks, A. P. Dove, H. Ding, R. K. O'Reilly, G. Chen and M. Jiang, *ACS Macro Lett.*, 2019, **8**, 596; (*c*) P. J. Hurst, A. M. Rakowski and J. P. Patterson, *Nat. Commun.*, 2020, **11**, 4690; (*d*) G. Virata and E. B. Gowd, *Polym. Chem.*, 2022, **13**, 838.

17 (*a*) B. Kalb and A. J. Pennings, *Polymer*, 1980, **21**, 607; (*b*) S. J. Organ, A. Keller and H. H. Wills, *J. Polym. Sci., Part B: Polym. Phys.*, 1986, **24**, 2319; (*c*) T. Y. Zhang, X. S. Guo, Z. K. Zhang, J. T. Xu and Z. Q. Fan, *Polymer*, 2020, **208**, 122979; (*d*) H. Abe, M. Harigaya, Y. Kikkawa, T. Tsuge and Y. Doi, *Biomacromolecules*, 2005, **6**, 457; (*e*) H. Ni'mahab and E. M. Woo, *CrystEngComm*, 2014, **16**, 4945; (*f*) S. Nurkhamidah and E. M. Woo, *J. Phys. Chem. B*, 2011, **115**, 13127.

18 C. Qiao, J. Zhao, S. Jiang, X. Ji, L. An and B. Jiang, *J. Polym. Sci., Part B: Polym. Phys.*, 2005, **43**, 1303.

19 (*a*) B. Lotz, T. Miyoshi and S. Z. D. Cheng, *Macromolecules*, 2017, **50**, 5995; (*b*) L. Jiang, T. Shen, P. Xu, X. Zhao, X. Li, W. Dong, P. Ma and M. Chen, *e-Polymers*, 2016, **16**, 1; (*c*) W. Xu, Y. Zheng and P. Pan, *J. Polym. Sci.*, 2022, **60**, 2136; (*d*) L. Liu, L. Zhu, Z. Chu and Z. Tong, *Macromolecules*, 2023, **56**, 5984.

20 (*a*) Y. Ge, Y. Wen, H. Liu, T. Lu, Y. Yu, X. Zhang, B. Li, S. T. Zhang, W. Li and B. Yang, *J. Mater. Chem. C*, 2020, **8**, 11830; (*b*) I. Yamazaki, N. Tamai and T. Yamazak, *J. Phys. Chem.*, 1987, **91**, 3572; (*c*) S. Karuppannan and J.-C. Chambron, *Chem. – Asian J.*, 2011, **6**, 964.

21 (*a*) G. K. Bains, S. H. Kim, E. J. Sorin and V. Narayanaswami, *Biochemistry*, 2012, **51**, 6207; (*b*) I. O. Aparin, G. V. Proskurin, A. V. Golovin, A. V. Ustinov, A. A. Formanovsky, T. S. Zatsepin and V. A. Korshun, *J. Org. Chem.*, 2017, **82**, 10015.

22 (*a*) Q. Song, S. Goia, J. Yang, S. C. L. Hall, M. Staniforth, V. G. Stavros and S. Perrier, *J. Am. Chem. Soc.*, 2021, **143**, 382; (*b*) V. Kumar, B. Sk, S. Kundu and A. Patra, *J. Mater. Chem. C*, 2018, **6**, 12086; (*c*) A. Fujii, Y. Sekiguchi, H. Matsumura, T. Inoue, W.-S. Chung, S. Hirota and T. Matsuo, *Bioconjugate Chem.*, 2015, **26**, 537.

23 (*a*) W. R. Algar, N. Hildebrandt, S. S. Vogel and I. L. Medintz, *Nat. Methods*, 2019, **16**, 815; (*b*) A. Rajak, C. K. Karan, P. Theato and A. Das, *Polym. Chem.*, 2020, **11**, 695; (*c*) L. Wu, C. Huang, B. P. Emery, A. C. Sedgwick, S. D. Bull, X.-P. He, H. Tian, J. Yoon, J. L. Sessler and T. D. Jame, *Chem. Soc. Rev.*, 2020, **49**, 5110.

24 P. Rajdev, D. Basak and S. Ghosh, *Macromolecules*, 2015, **48**, 3360.